Compensated right ventricular function of the onset of pulmonary hypertension in a rat model depends on chamber remodeling and contractile augmentation

Daniela Vélez-Rendón[1], Xiaoyan Zhang[2], Jesse Gerringer[1,3] and Daniela Valdez-Jasso[1,2]

[1]Department of Bioengineering, University of Illinois at Chicago, Chicago, IL, USA; [2]Department of Bioengineering, University of California San Diego, La Jolla, CA, USA; [3]Department of Biomedical Engineering, Marquette University, Milwaukee, WI, USA

Abstract

Right-ventricular function is a good indicator of pulmonary arterial hypertension (PAH) prognosis; however, how the right ventricle (RV) adapts to the pressure overload is not well understood. Here, we aimed at characterizing the time course of RV early remodeling and discriminate the contribution of ventricular geometric remodeling and intrinsic changes in myocardial mechanical properties in a monocrotaline (MCT) animal model. In a longitudinal study of PAH, ventricular morphology and function were assessed weekly during the first four weeks after MCT exposure. Using invasive measurements of RV pressure and volume, heart performance was evaluated at end of systole and diastole to quantify contractility (end-systolic elastance) and chamber stiffness (end-diastolic elastance). To distinguish between morphological and intrinsic mechanisms, a computational model of the RV was developed and used to determine the level of prediction when accounting for wall masses and unloaded volume measurements changes. By four weeks, mean pulmonary arterial pressure and elastance rose significantly. RV pressures rose significantly after the second week accompanied by significant RV hypertrophy, but RV stroke volume and cardiac output were maintained. The model analysis suggested that, after two weeks, this compensation was only possible due to a significant increase in the intrinsic inotropy of RV myocardium. We conclude that this MCT-PAH rat is a model of RV compensation during the first month after treatment, where geometric remodeling on EDPVR and increased myocardial contractility on ESPVR are the major mechanisms by which stroke volume is preserved in the setting of elevated pulmonary arterial pressure. The mediators of this compensation might themselves promote longer-term adverse remodeling and decompensation in this animal model.

Introduction

Pulmonary arterial hypertension (PAH) is a severe disease of the pulmonary vasculature that is characterized by a resting mean pulmonary arterial pressure (mPAP) ≥ 25 mmHg with a pulmonary arterial wedge pressure ≤ 15 mmHg.[1] During the development of PAH, the right ventricle (RV) of the heart becomes subjected to pressure overload, which results in chamber remodeling that initially compensates for the increase in pulmonary vascular resistance (PVR). Eventually this response becomes maladaptive and, if left untreated, PAH results in cardiac decompensation and heart failure.[2] Prior investigations in PAH patients have indicated that increased RV diastolic stiffness is related to adverse clinical outcomes[3] and reduced survival.[4] However, the process of remodeling and adaptation that the RV undergoes in response to pulmonary pressure overload is

Corresponding author:
Daniela Valdez-Jasso, 9500 Gilman Drive, PFBH 429, La Jolla, CA 92093-0412, USA.
Email: dvaldezjasso@ucsd.edu

not clear, making it harder to determine when the RV goes from adapting to failure.

To relate pulmonary hemodynamics to right ventricular mechanics and thereby better characterize the time course of RV early remodeling during PAH, we carried out a longitudinal study in an animal model of PAH. Using invasive measurements of RV pressure and volume in a monocrotaline (MCT) animal model of PAH, ventricular morphology and function were assessed weekly during the first four weeks after MCT exposure. To test whether the observed changes in right ventricular diastolic and systolic function could be explained by the observed changes in right ventricular preload, afterload, and wall geometry alone, we compared measured RV pressure-volume (PV) end-diastolic and end-systolic relations with those predicted by a computational model that included measured geometrical chamber remodeling.

RV systolic and diastolic pressures rose significantly after the second week of PAH induction accompanied by significant RV hypertrophy, but RV stroke volume (SV) and cardiac output (CO) were maintained. The model analysis suggested that, after two weeks, this compensation was only possible due to a significant increase in the intrinsic inotropy of RV myocardium.

Methods

Animal preparation

All experiments were performed with the approval of the Animal Care and Use Committee at the University of Illinois, Chicago. The study included 45 male Sprague Dawley rats weighing 275 ± 12 g (Charles River, Chicago, IL, USA). PAH was induced in the treatment group by a subcutaneous injection of 60 mg/kg of monocrotaline (crotaline, Sigma-Aldrich). The longitudinal study of PAH was carried out by weekly evaluations of the RV-PA hemodynamics for up to four weeks post injections. The treated rats studied after one week of the injection (PAH1) represent the early stage whereas the group studied after four weeks of receiving the injection (PAH4) corresponds to the late stage of PAH. A control group was injected with saline matching the volumetric dose of the treated group. To account for the aging effects, the control group ($N_{CTL} = 7$) consisted of animals injected after one, two, three, or four weeks ($N_{CTLweek1} = 1$, $N_{CTLweek2} = 2$, $N_{CTLweek3} = 3$, $N_{CTLweek4} = 1$). When possible, a treated PAH animal was paired with a control (CTL) animal and housed together for up to four weeks. The group sizes for each disease stage were $N_{PAH1} = 8$, $N_{PAH2} = 8$, $N_{PAH3} = 6$, and $N_{PAH4} = 16$.

In-vivo hemodynamic studies

The paired rats underwent surgery the same day, one after another. The animals were anesthetized using isoflurane (Henry Schein, NY, USA). Anesthesia was initially administered by placing the animal in an induction chamber supplied with oxygen mixed with 4% isoflurane. When the animal was confirmed to be unconscious, the anesthesia was decreased to 2.5% and supplied via a nasal cone. Following a tracheotomy, the rat was intubated (E-Z Anesthesia Ventilation System, Palmer, PA, USA) and supplied with a respiratory rate of 50 breaths per minute and a tidal volume based on the animal's weight.[5] The heart and great vessels were exposed via a thoracotomy. Once the chest cavity was opened and the RV was identified, a 21-gauge needle was used to puncture the ventricular wall apically. The needle was immediately replaced by a 1.9F PV admittance catheter (Transonic Scisense, ON, Canada) introduced along the long axis of the chamber. Once PV waveforms recorded were reproducible in steady state (steady-state conditions), the inferior vena cava (IVC) was slowly occluded with a suture line (Fine Science Tools Braided Silk Suture 5-0, Foster City, CA, USA) for a few seconds to change the venous return (occlusion conditions). On average, five occlusions were performed on each animal. Following PV measurements, a second puncture was made on the RV base next to the outflow track using a 23-gauge needle. A 1.6-F dual-pressure sensor catheter (Transonic Scisense, ON, Canada) was inserted into the RV and advanced into the main pulmonary artery (MPA) via the pulmonic valve for simultaneous measurements of the RV and MPA pressures. The MPA pressure time series was used to calculate mPAP and thus confirm PAH. At the conclusion of the hemodynamic measurements, the animals were exsanguinated and the heart and lung vessels were flushed with phosphate buffered saline (PBS; 0.14M NaCl; 0.0027M KCl; 0.0017M KH_2PO_4; 0.01M Na_2HPO_4) and heparin (Fresenius Kabi, USA). Data were collected in LabChart Software (AD Instruments Inc., Version 8.0 Pro, Colorado Springs, CO, USA).

Hemodynamic metrics such as SV, ejection fraction (EF), heart rate (HR), CO, total PVR, and ventricular relaxation time constant τ were computed through a custom-written MATLAB (Mathworks Inc, Version 8.6.0, Natick, MA, USA) code. The end-systole (ES) point was determined by finding the maximum value of the pressure to volume ratio in a given pressure-volume loop. The end-diastole (ED) point was the first point in the pressure-volume loop with highest volume and lowest volume rate of change (i.e. dV/dt $\sim$0). Based on the difference in volume at ED and ES, SV was calculated. EF was determined by the ratio of SV and ED volume. Using the calculated SV and HR, CO was computed by taking the product of the two. Total PVR was computed as the ratio between RV ES pressure and CO.[6] The RV relaxation time τ was calculated by fitting an exponential decay function to the pressure waveform $p(t) = P_\infty + (P_0 - P_\infty)e^{-\frac{t}{\tau}}$ from the point dP/dt$_{min}$ occurs until the end of systole (or when the pulmonic valve closes). Here the zero-asymptote assumption is neglected. Instead, P_0 is the pressure at time of dP/dt$_{min}$ and P_∞ the pressure of a fully relaxed ventricle held at its end-systolic

volume.[7,8] To quantify ventricular hypertrophy, the RV weight was normalized to the sum of the left ventricle and septum weight (Fulton index[6]). Hypertrophy of the RV was considered established if the Fulton index ratio was > 0.25.[9] RV wall thickness was measured in three different locations along the wall using a thickness gauge (1010Z, Starrett, Athol, MA, USA, with a range of 0–0.375" and accuracy of ± 0.001"") and averaged for each animal.

Right-ventricular and pulmonary vascular elastances

Ventricular contractility or end-systolic elastance E_{es} corresponds to the slope of the linear regression to the end-systolic points during occlusion of the IVC (approximately 40% drop in blood pressure). Based on the steady-state PV measurements, the effective pulmonary arterial elastance E_a or the slope of the line between the ES point and ED volume at zero pressure was obtained. E_a is a parameter that relates to the ability of the pulmonary vasculature to buffer the incoming blood pressure and volume influx. By taking the ratio of E_{es} and E_a, the ventriculo-vascular coupling η can be assessed.[10] Finally, passive ventricular chamber stiffness was calculated by fitting the ED PV data points during occlusion of the IVC using the following exponential

function $P(V) = \gamma e^{\beta V}$. Here, β is the diastolic stiffness constant and γ is a curve fitting constant. End-diastolic elastance E_{ed} was determined by evaluating chamber stiffness ($dP/dV = \gamma \beta e^{\beta V}$) at the ED point during PV steady-state conditions.

Relating ventricular pressure-volume to ventricular wall mechanics at ES and ED

To compute RV end-diastolic and end-systolic pressure-volume relations from RV geometry and myocardial resting and active material properties, a spherical model of the RV was developed. The RV model comprehends the RV cavity, RV free wall, and septum. Assuming that the RV is a fraction of a sphere with an outer radius R, the volume of the sphere is the sum of the RV free wall volume V_w, the septum volume V_{sw}, and the RV cavity volume V_{RV}, viz.,

$$k_r \frac{4}{3}\pi R^3 = V_w + V_{RV} + V_{sw} \quad (1)$$

This formulation assures that the radius of the cavity is not zero when the RV volume V_{RV} is zero. The fraction of

Table 1. Summary statistics of hemodynamics, elastances, and RV structural changes observed during PAH progression.

Parameter	CTL (n = 7)	PAH1 (n = 8)	PAH2 (n = 8)	PAH3 (n = 6)	PAH4 (n = 4)
Fulton Index	0.24 ± 0.04	0.31 ± 0.05	0.34 ± 0.04*	0.47 ± 0.1*,†,‡	0.52 ± 0.03*,†,‡
RV weight (g)	0.22 ± 0.04	0.23 ± 0.04	0.3 ± 0	0.37 ± 0.05	0.47 ± 0.05*,†
RV thickness (mm)	0.61 ± 0.08	0.59 ± 0.1	0.6 ± 0.08	1.03 ± 0.07*,†,‡	1.12 ± 0.12*,†,§
Animal's weight (g)	268 ± 23.3	262.1 ± 43.2	293 ± 18.1	267.3 ± 24.6	283.7 ± 24.9
ESP (mmHg)	31.7 ± 6.1	27.3 ± 2.4	39.5 ± 6	52.3 ± 7.3†	70.5 ± 6.8*,†
ESV (µL)	90.8 ± 19.3	79.2 ± 19.3	109.7 ± 37	126.1 ± 25.9	140.9 ± 35.6†
EF (%)	62.3 ± 6.7	64.2 ± 6.4	61 ± 7.6	53.6 ± 9.9	53.9 ± 5.4
CO (mL/min)	41.2 ± 3.5	40.5 ± 8.4	51.7 ± 10.8	45.9 ± 13.5	45.5 ± 3.4
SV (µL)	149 ± 16.7	141.1 ± 22.9	165.9 ± 24.5	148.3 ± 38.3	160.3 ± 6
dP/dt_{max} (mmHg/µL)	1603.8 ± 316.2	1492.4 ± 242.4	1933.4 ± 394.8	2082.6 ± 123.9†	2680.3 ± 311.5*,†,‡
HR (bpm)	278.5 ± 26	286.7 ± 40.7	311.2 ± 39.2	307.4 ± 17.5	284.2 ± 23.6
mPAP (mmHg)	24.3 ± 4.9	25.2 ± 2	32.6 ± 4.8*	34.3 ± 4.6*	42.8 ± 4.9*,†,‡
Total PVR (mmHg/mL.min)	0.8 ± 0.2	0.7 ± 0.2	0.8 ± 0.2	1.2 ± 0.4	1.6 ± 0.2†
EDP (mmHg)	4.6 ± 0.7	3.5 ± 1.4	4.6 ± 1.4	5.4 ± 2.3	7.7 ± 1.7†,‡
EDV (µL)	239.7 ± 19.6	220.3 ± 31.6	275.6 ± 49.5	274.4 ± 36.7	301.3 ± 37.8†
dP/dt_{min} (mmHg/µL)	-1274 ± 349.4	-1079.2 ± 172.3	-1462.6 ± 308.2	-1876.9 ± 233.7*,†	-2080.6 ± 237.7*,†,‡
τ (ms)	15.1 ± 3.4	13.6 ± 2.8	14.7 ± 4	12.8 ± 1.4	11.1 ± 3.4
E_{es} (mmHg/µL)	0.25 ± 0.08	0.25 ± 0.11	0.25 ± 0.09	0.34 ± 0.1	0.45 ± 0.13*,†,‡
E_a (mmHg/µL)	0.2 ± 0.06	0.21 ± 0.06	0.24 ± 0.04	0.4 ± 0.16	0.42 ± 0.07*,†
E_{ed} (mmHg/µL)	0.03 ± 0.013	0.015 ± 0.006	0.019 ± 0.011	0.027 ± 0.023	0.033 ± 0.005
η	1.31 ± 0.52	1.25 ± 0.67	1.05 ± 0.39	1.06 ± 0.6	1.11 ± 0.3

*$P < 0.05$ vs. CTL.
†$P < 0.05$ vs. PAH1.
‡$P < 0.05$ vs. PAH2.

the sphere k_r that best matched the measured mean RV masses and wall thickness (Table 1) was found to be 0.6. V_w and V_{sw} were computed using the measured RV wall mass and 45% of the LV wall mass divided by myocardial density 1.053 g/mL.[11] The 45% is an estimate of the LV wall mass occupied by the septal wall based on experimental observations. Sensitivity analysis of the geometric parameters k_r, which was in the range of 0.4–0.8 and septum wall percentage of 25–60%, were found not to affect the final conclusions drawn from this model.

At the unloaded volume, $V_{RV} = V_0$ and $R = R_0$, so that

$$R_0 = \sqrt[3]{\frac{V_0 + V_w + V_{sw}}{k_r \frac{4}{3}\pi}} \qquad (2)$$

V_0 was estimated from the *in-vivo* measurements. Based on the assumption that ED pressure at V_0 is zero and the physiological constraint of V_0 being positive at ED, the measured ED pressure was normalized, i.e. the minimum ED pressure value was subtracted from the raw data. Hence, V_0 was estimated to be the mean value of volumes at zero ED pressure.

The radius R and wall thickness h of the spherical model in terms of V_0 and R_0 are computed as:

$$R = R_0 \sqrt[3]{\frac{V_w + V_{RV} + V_{sw}}{V_0 + V_w + V_{sw}}}, \quad and \quad h = \frac{V_w}{k_r 4\pi R^2} \qquad (3)$$

To avoid over-restricting the model geometry, the experimentally measured wall thickness was not directly incorporated in the computational modeling. Instead, Eq. 3 for wall thickness was used. A schematic of the model is illustrated in Fig. 1.
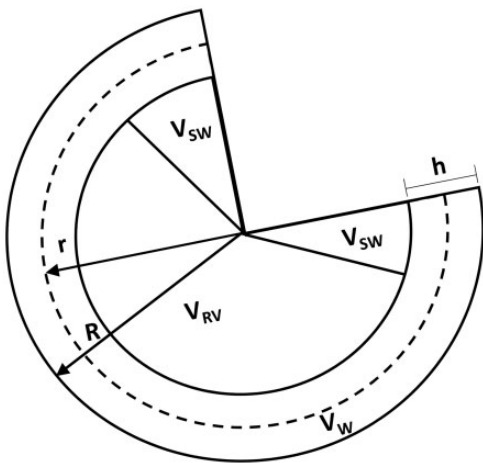

Fig. 1. Schematic of the RV computational model modeled as a fraction of a sphere of outer radius R and mid-wall radius r. In a cross-section of the sphere, the RV cavity V_{RV}, RV free wall V_w, and septum V_{sw} volumes illustrate the different compartments of the RV model.

For sarcomere mechanics,[12] the myocardium passive stress was defined as

$$T_p = k_1\left(e^{k_2(\lambda-1)} - 1\right) \quad \text{where} \quad \lambda = \frac{L_s}{L_R} = \frac{r}{r_0} \qquad (4)$$

k_1 and k_2 are material parameters, where k_1 is a stiffness coefficient. λ is the stretch ratio of sarcomere length L_s to reference length ($L_R = 1.95\,\mu m$) measured from the mid-wall radius $r = R - \frac{h}{2}$. Based on the model used by Guccione et al.'s work, the myocardium active stress at ES[13,14] was defined as follows

$$T_a = T_{max} \frac{Ca_0^2}{Ca_0^2 + \frac{Ca_{max}^2}{e^{B(L_s - L_0)} - 1}} \qquad (5)$$

where T_{max} is maximal isometric tension achieved at the longest sarcomere length and maximum peak intracellular calcium concentration ($Ca_{max} = 4.35\,\mu M$).[13] Ca_0, set to $0.25\,\mu M$, is the peak intracellular calcium concentration, L_0 or $1.50\,\mu m$ is the sarcomere length at which no active tension develops, and B is the scale that determines the shape of peak isometric tension-length relation. The material parameters of the resting and active sarcomere length-tension relations L_0, L_R, L_s, Ca_o, and Ca_{max} were constrained to previously measured constants, and k_1, k_2, T_{max}, and B were determined by fitting the model to measured RV PV relations.

Given that the RV wall is thin compared to its cavity radius,[15] the thin-walled LaPlace's law was used to estimate mean mid-wall stresses. Here, the RV cavity blood pressure P is computed as

$$P = \frac{2Th}{r}$$

where the ventricular wall stress T is the sum of the active and passive stress ($T = T_a + T_p$) generated at the sarcomere length, L_s. For EDPVR, the total tension equals passive tension (i.e. no active tension at ED).

To predict ESPVR and EDPVR, PV data from each individual animal obtained during IVC occlusions were fitted using the linear and exponential functions described in the previous section. Using the fitted functions corresponding to each individual animal over a common pressure and volume range, a mean ± standard error curve was generated to represent the measured data per group. While keeping the parameters L_0, L_R, Ca_0, and Ca_{max} constant, the material property parameters $\theta^C = \{k_1^C, k_2^C, T_{max}^C, B^C\}$ were adjusted to match the ESPVR and EDPVR interpolated data of the control group. The values of θ^C were initialized based on reported values and modified while assuring that the resultant length-stress relationship was within the physiological ranges reported for rat RV by ter Keurs et al.[16] The geometric variables V_w, V_{sw}, and V_0 were measured directly in our experiments or derived directly from measurements

using relationships given here. The RV model with different geometries for each group was reflected by different V_0 and wall masses (V_w, V_{sw}), first with the control group material parameters θ^C, and then with a new set of adjusted material parameters. All the RV computational model calculations were carried out in Python computing environment (version 3.6).

Statistical analysis

Descriptive statistics were computed for all the hemodynamic measurements, RV tissue measurements, and elastances. To detect significant differences among groups, non-parametric Wilcoxon/Kruskal–Wallis (Chi-square approximation) tests were conducted in cases where observations displayed departures from a normal distribution; otherwise, parametric analysis of variance was carried out. When a difference in treatment was found to be significant, multiple group comparisons were then conducted to identify where the differences occurred between the groups (CTL, PAH1, PAH2, PAH3, PAH4). Multiple comparisons Tukey HSD were used for the normally distributed data; otherwise the Dunn Method was implemented. All the statistical analyses were carried out in JMP Pro Statistical Software (version 13.0.0, © SAS Institute Inc., Cary, NC, USA). For all statistical tests, significance level was set at 0.05. All values are presented as mean ± standard deviation, unless specified.

Results

Animal preparation

Out of 38 animals administered with MCT, 26 developed PAH. Two animals were normotensive, four unexpectedly died at the beginning of the surgical procedure unable to confirm PAH, and six died between weeks 3 and 4 post injection. RV samples and weights were collected from the 19 out of 26 treated and six out of seven control animals.

In-vivo hemodynamics

The PV loops from each group exhibited unique hemodynamic characteristics. The CTL group exhibited a square-shape loop through the four weeks with tight systolic pressure (31.7 ± 6.1 mmHg) and volume ranges (90.8 ± 19.3 to 239.7 ± 19.6 µL). In the case of the treated animals, RV ES pressures rose each week from 27.3 ± 2.4 up to 70.5 ± 6.8 mmHg (P value $= 0.0004$). ED pressures also increased, significantly in the late PAH group (from 3.5 ± 1.4 to 7.7 ± 1.7 mmHg, P value $= 0.028$, PAH4 vs. PAH1). While the width of the PV loops or SV remained statistically the same (from 141.1 ± 22.9 to 160.3 ± 6 µL), there was a shift to the right of ES volume (from 79.2 ± 19.3 to 140.9 ± 35.6 µL, P value $= 0.0190$) and ED volume (from 220.3 ± 31.6 to 301.3 ± 37.8 µL, P value $= 0.0189$) as

weeks advanced, indicating the enlargement of the ventricle and an increase in resting volume. CO was also maintained in disease and remained statistically the same for all groups. The increase in mPAP (from 25.2 ± 2 to 42.8 ± 4.9 mmHg, P value $= 0.0001$) and total PVR (from 0.7 ± 0.2 to 1.6 ± 0.2 mmHg/mL min, P value $= 0.0149$) was reflected in the PV loop shape by producing the formation of a shoulder during the ejection phase (slanted/triangular shape). The increase in ED volume and preserved SV caused a slight decrease in EF ($64.2 \pm 6.4\%$ to $53.9 \pm 5.5\%$). Ventricular diastolic function parameters dP/dt_{min} and τ decreased, with a statistically significant difference only found for dP/dt_{min} at the late disease stages (vs. normotensive and early PAH, $P < 0.0001$). Summary statistics of the hemodynamic measurements are shown in Figs. 2 and 3 and Table 1.

Right-ventricular morphology

Right ventricular morphology changed with the progression of the disease (Fig. 2). The ventricle progressively became hypertrophic (Fulton index from 0.31 ± 0.05 to 0.52 ± 0.03, P value $= 0.0011$, RV weight from 0.23 ± 0.04 to 0.47 ± 0.05 g, P value $= 0.0316$) and thickened significantly (from 0.6 ± 0.1 mm in the normotensive group to 1.1 ± 0.1 mm in advanced PAH, P value < 0.0001) by week 2 post treatment. The weight of the animals, however, remained the same.

Right-ventricular and pulmonary vascular elastances

Effective arterial elastance E_a significantly increased at the late PAH stages (PAH3 and PAH4 groups). E_{es} initially did not change (CTL, PAH1, and PAH2 groups) but then increased significantly in the PAH3 group (0.25 ± 0.08 to 0.34 ± 0.1 mmHg/µL, P value $= 0.0435$) and further increased in PAH4 (0.45 ± 0.13 mmHg/µL, P value $= 0.0460$ vs. CTL). End-diastolic elastance E_{ed} dropped initially (CTL: 0.030 ± 0.01 to PAH1: 0.015 ± 0.006 mmHg/µL), but then progressively increased reaching baseline value at week 4 (0.033 ± 0.005 mmHg/µL). γ and β were not statistically different across the groups. γ was unaffected at the early PAH stages and displayed an increase after three weeks of MCT treatment. Diastolic chamber stiffness β, on the other hand, decayed in the first week of MCT treatment and remained overall constant until late PAH. The RV and pulmonary system remained coupled during the progression of PAH. This was reflected in the ventricular-vascular coupling efficiency η, which was not statistically different among the treatment groups. E_{es}, E_a, E_{ed}, and η are summarized in Fig. 4.

Ventricular hemodynamics related to ventricular wall mechanics at ES and ED

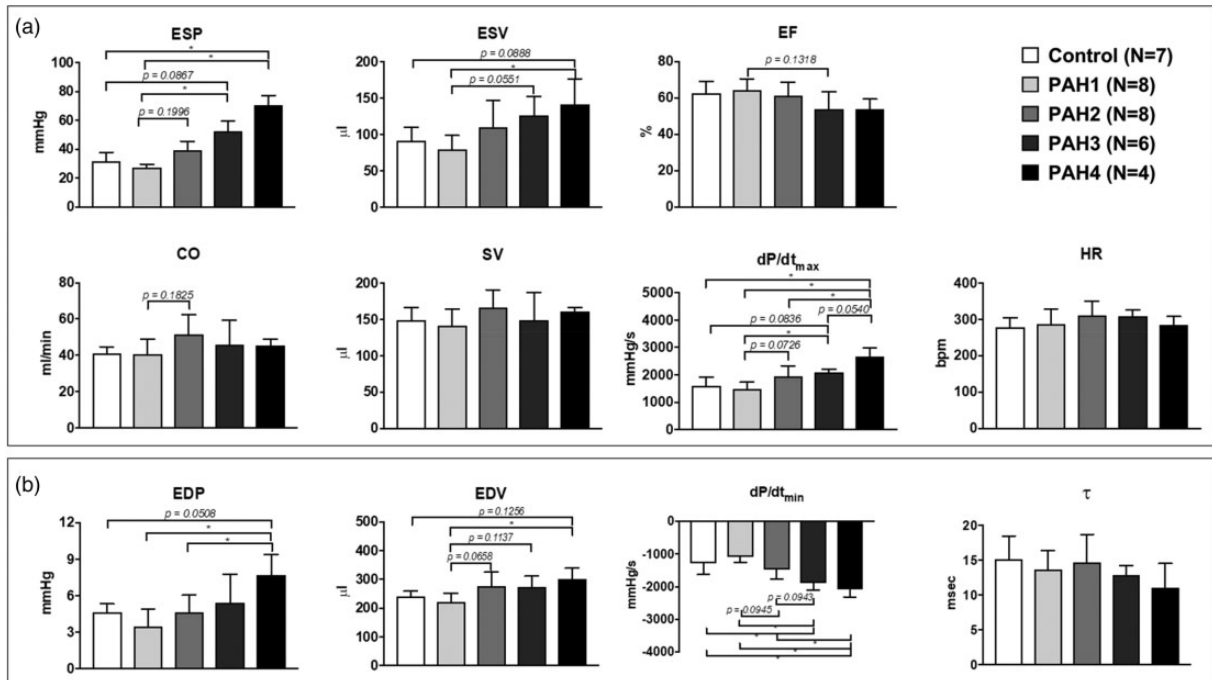The RV model was able to recapitulate the experimentally measured mean RV pressure-volume relations at ES and ED

Fig. 2. Summary statistics of cardiac performance during systole (a) and diastole (b). *$P < 0.05$.
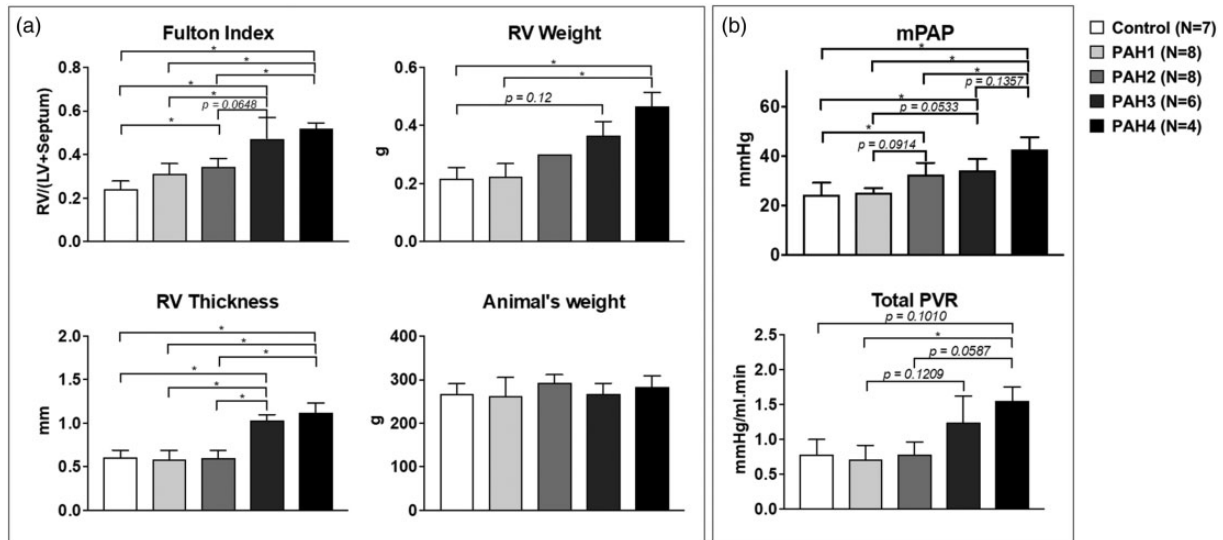

Fig. 3. Summary statistics of RV hypertrophy evidenced with Fulton Index, RV thickness, and RV weight. (a) No changes in animal weights are shown. (b) mPAP and total PVR. *$P < 0.05$.

(Fig. 5a, left). Using geometric measurements from PAH groups (solid lines), the RV model with the control-group material properties overestimated EDPVR at week 1, closely matched the mean EDPVRs measured in the PAH groups at weeks 2 and 3, and underestimated EDPVR at week 4. The ESPVR model predictions were highly underestimated for the week 2, 3, and 4 PAH groups. However, when accounting for the geometrical changes and adjusting the material properties k_1 and T_{max} to increase intrinsic myocardial passive and active tension development, predictions from the model (dashed line) all showed good agreement with experimentally measured mean ESPVRs across the ranges of volumes measured in the PAH groups. Similar findings and the same conclusions were obtained when the entire analysis was repeated with altered assumed fraction of septal wall in the LV wall mass. Model parameters are shown in Table 2, with the adjusted k_1 and T_{max} values to account for a given PAH group material properties.
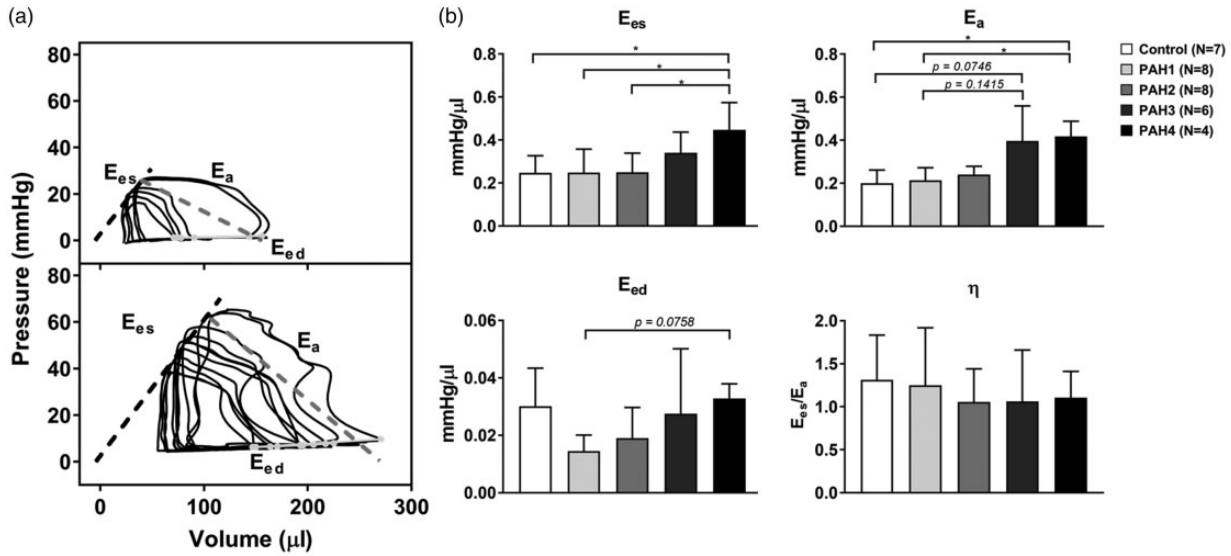
Fig. 4. (a) Representative occlusion PV loops of control and after 4 weeks of MCT administration (chronic PAH). Ees: slope of dashed black line (ESPVR); E_a: slope with dashed dark gray line; E_{ed}: slope with light gray line. (b) Summary statistics of E_{es}, E_a, E_{ed}, and η are also depicted. *$P < 0.05$.
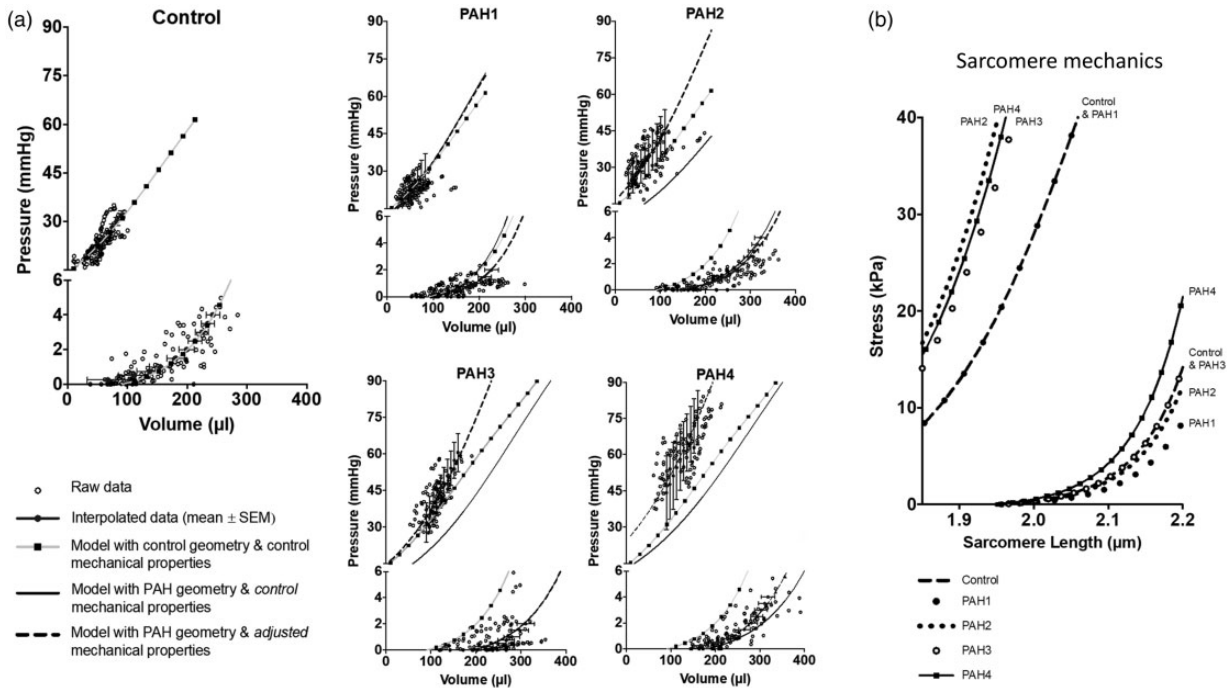

Fig. 5. (a) Comparison of measured raw (open circles) and averaged (blue dots and bars) right-ventricular end-diastolic and end-systolic pressure-volume relations with computational model predictions. Control: Model-predicted end-diastolic and end-systolic PV relations (squares and gray lines) using control-group geometry and control-matched material properties. PAH1-4: Model-predicted end-diastolic and end-systolic PV relations (squares and gray lines) using control-group geometry and control material properties. Model-predicted end-diastolic and end-systolic PV relations (solid lines) using PAH geometry and control material properties. Model-predicted end-diastolic and end-systolic PV relations (dashed lines) using PAH geometry and PAH-matched material properties. (b) Model-predicted isometric end-systolic and end-diastolic sarcomere length-tension relations for all 5 animal groups determined by optimizing material parameters to match measured RV pressure-volume relations. Note the increase in predicted systolic sarcomere elastance 2–4 weeks after MCT. End-diastolic sarcomere stiffness tension decreases at week 1 of PAH and increases by.

Table 2. Parameters used in the computational model of the RV to predict PV relations at end-systole and end-diastole.

Parameter	CTL (n = 7)	PAH1 (n = 8)	PAH2 (n = 8)	PAH3 (n = 6)	PAH4 (n = 4)
V_0 (μL)	91.76	106.25	152.39	195.55	185.87
V_w (μL)	209	218	218	351	446
V_{sw} (μL)	385	308	376	321	385
k_1^c (mmHg)	2.3	2.3	2.3	2.3	2.3
k_1 (mmHg)	–	1.4	2.0	2.3	3.5
k_2^c	30	30	30	30	30
T_{max}^c (mmHg)	640	640	640	640	640
T_{max} (mmHg)	–	640	1300	1100	1200
B^c (μm^{-1})	10	10	10	10	10

The morphology parameters V_0, V_w, V_{sw} are the unloaded volumes, RV free wall volume, and volume of septum wall, respectively. The material property parameters $\theta^C = \{k_1^C, k_2^C, T_{max}^C, B^C\}$ are based on the model predictions of ES PV and ED PV of the control animals. When changes in morphology did not match ESPVR and EDPVR, this gave rise to a new set of adjusted material properties – in this case, k_1 and T_{max}.

Based on the RV model predictions of ESPVR and EDPVR with the adjusted parameters (Table 2), active and passive sarcomere length-stress curves were generated for each treatment group. As shown in Fig. 5b, the control, PAH2 and PAH3 passive length-stress curves closely overlap. However, there was a decrease in muscle stiffness in PAH1 (from $k_1 = 2.3$ to 1.4 mmHg) and a large increase in muscle stiffness at PAH4 (from $k_1 = 2.3$ to 3.5 mmHg). The active sarcomere length-stress relation in the control and PAH1 groups were the same. However, this relation changed for the PAH2 group, where the contractility of the muscle increased—from $T_{max} = 640$ to 1300 mmHg— and remained high ($T_{max} = 1100$ and 1200 mmHg) in the following weeks.

To discriminate the contributions of RV geometric remodeling from changes in diastolic and systolic myocardial material properties on the preservation of RV SV, the model was used to compute RV end-diastolic and end-systolic pressure-volume relations using three combinations of model geometry and material properties (Fig. 6): control-group geometry and material properties (dotted lines in Fig. 6b); PAH geometries and control material properties (solid lines in Fig. 6b); PAH geometries and PAH material properties (dashed lines in Fig. 6b). From these computed ED and ES PV relations, SVs were computed to quantify how the changes in hemodynamics, wall geometry and passive and active myocardial material properties combined to maintain CO in the presence of altered RV hemodynamics.

The SV labeled SV_1 in Fig. 6b represents the SV predicted under PAH loading conditions if there had been no geometric remodeling or changes in myocardial diastolic or systolic material properties. Without compensatory changes in ventricular geometry, elastic and contractile properties, the steep decrease in SV_1 indicates that right ventricular function would have been reduced by 75% after four weeks, and that elevated RV EDP had not been sufficient to compensate

after week 1. SV_2 is the SV computed when the contribution of geometric remodeling on the EDPVR was accounted for in the models. It shows that RV dilation after week 1 was a major contributor to the preservation of RV SV. The contribution of altered geometry and diastolic compliance on the EDPVR is represented by SV_3. The transient decrease in RV myocardial stiffness was the major compensatory mechanism at week 1, but after week 1, the contribution of altered RV passive stiffness was minor and actually negative as the myocardial stiffness increased by week 2. SV_4 represents the contribution to maintenance of SV of diastolic material and chamber remodeling and the effects of geometric remodeling on the ESPVR. Subtracting SV_3 shows that the effects of changes in ventricular geometry on the ESPVR actually worked slightly against compensation. The increase in ventricular radius that increased ED volume was not fully overcome by the increase in RV wall thickness. Finally, when the effects on SV of chamber remodeling and diastolic and systolic material properties on both the EDPV and ESPV relations were all included in the model (SV_5), the additional effect of increased contractility was also shown to be an important compensatory mechanism. In summary, the effects of geometric remodeling on the EDPVR and of increased myocardial contractility on the ESPVR were the major mechanisms by which SV was preserved in the setting of elevated PAP, and both mechanisms contributed equally during weeks 2–4. In week 1, the minor loss of SV that the modest hemodynamic changes would have caused was fully compensated by a transient decrease in diastolic myocardial stiffness before any geometric remodeling or contractile compensation had begun.

Discussion

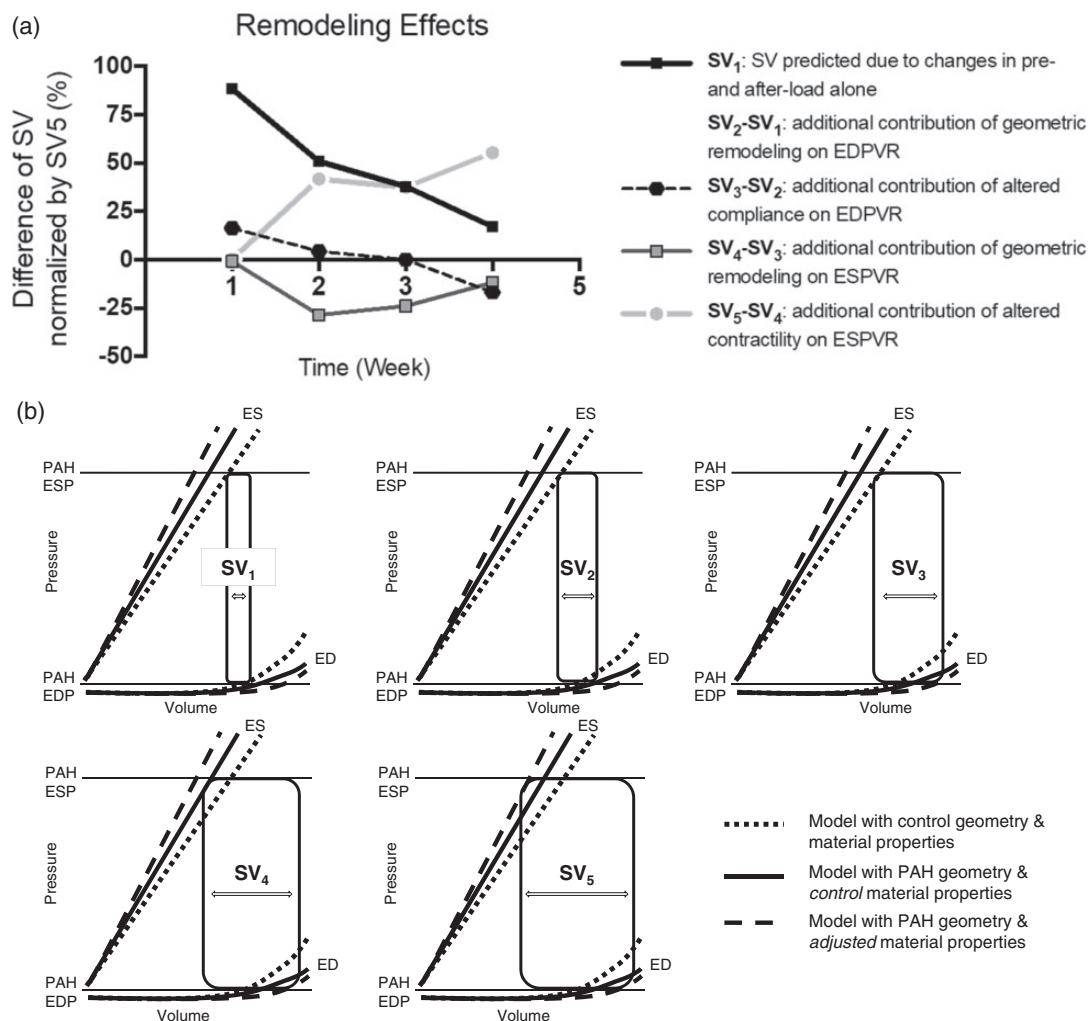In the present study, RV hemodynamic and morphological measurements were taken to investigate the compensated

Fig. 6. (a) Model-predicted changes in RV SVs from weeks 1–4 due to: (SV_1) changes in preload and afterload only; (SV_2–SV_1) the additional contribution of geometric remodeling on the EDPVR; (SV_3–SV_2) the further contribution of altered diastolic compliance on the EDPVR; (SV_4–SV_3) the further contribution of geometric remodeling on the ESPVR; (SV_5–SV_4) the further contribution of altered contractility on the ESPVR. (b) Graphical definitions of model-predicted SVs SV_1–SV_5 obtained from model-predicted EDPVR and ESPVR computed using: control-group geometry and control-group material properties (dotted lines); PAH geometries and control material properties (solid lines); PAH geometries and PAH material properties (dashed lines).

phase of RV hypertrophy in the MCT-animal model of PAH. Our goal was to discriminate the contributions of ventricular geometric remodeling and intrinsic changes in myocardial mechanical properties at ES and ED to the maintenance of CO using a computational model. In this longitudinal study, the myocardium was found to initially decrease its stiffness—an acute adaptation that preserved SV at week 1 of PAH induction and reversing by week 2. This transient early decrease in diastolic stiffness allowed the RV to soften initially in order to preserve diastolic filling and therefore maintain SV. By week 2, the PAP, PVR, and end-systolic volume all increased while maintaining SV, CO, and EF. This compensated response could be explained in the model almost entirely by the changes in chamber volume and mass. However, after week 2, the changes in RV volume and wall thickness and increased filling were not sufficient to maintain SV and CO as PAP continued to increase. This led us to conclude that there was a significant increase in RV contractility during this period as shown by the increased T_{max} values required to match the experiment-derived ESPVR. Furthermore, this MCT-PAH rat is a model of RV compensation during the first month after treatment, where geometric remodeling on EDPVR and increased myocardial contractility on ESPVR are the major mechanisms by which SV is preserved in the setting of elevated PAP. The mediators of this compensation might themselves promote longer-term adverse remodeling and decompensation in this animal model.

MCT-model of PAH shows features of preserved cardiac function

In our study, RV pressures rose and volumes increased while maintaining CO, SV, and EF. Our results are in agreement with Handoko et al.,[17] where CO was preserved in rats with no significant difference in total PVR by day 14 after MCT injections. In their study, like ours, by day 28 after MCT injections, there was a significant increase in total PVR while CO continued to be preserved. Yin et al. also reported maintenance of EF and CO in their four-week of MCT-rat model.[18] In addition to CO being preserved, Werchan et al. also measured significant decrease (more negative values) in dP/dt_{min} in four-week MCT-treated rats.[19] Like Werchan et al., magnitude of the rate of pressure change during relaxation (dP/dt_{min}) became significantly more negative, but relaxation time τ only slightly decreased in advanced PAH. This discrepancy has been previously reported by Umar et al., where no change in the relaxation time τ was found in the presence of an increasing trend in dP/dt_{min} magnitude[20] or vice versa by Correia-Pinto et al. in MCT-induced PAH rats.[21] These findings suggest that in the four-week MCT model, the RV maintains diastolic functional elasticity and is still in a compensatory phase. The work by Handoko et al. showed that after these four weeks, there is a statistically significant decline in CO, indicating the end of the RV compensation phase.

Sudden deaths between week 3 and week 4 after MCT injections occurred in our study. MCT is a toxic alkaloid that when ingested produces a syndrome characterized by pulmonary hypertension, pulmonary vasculitis, and RV hypertrophy.[22] To date, the toxicological mechanisms of the MCT in the lung are unknown. Abe et al. have suggested that MCT-injected rats probably die of cardiac and renal dysfunction.[23] In a study by Umar et al. they reported sudden death in their 30% death rate 23 days after MCT injections and 100% by day 32 post injections, attributing this to spontaneous ventricular fibrillation.[24] Several groups have reported varying rates after three weeks of treatment.[25–28] Some prominent studies indicate the presence of a proarrhythmic substrate in hearts of MCT-treated rats, and among the causes of sudden death are the changes in Ca^{2+} and K^+ channel activity and electrical restitution.[29–32]

Pulmonary arterial stiffness increases in late PAH

Pulmonary arterial stiffening markedly increased and became significantly different from the control group to the MCT-injected rats after three weeks. Pulmonary arterial elastance E_a values increased as PAH advanced, which has also been reported by other groups when using the rat MCT model: Yin et al. from 0.5 ± 0.14 to 0.79 ± 0.3 mmHg/μL;[18] and de Man et al. from 0.15 to 1.0 mmHg/μL.[33] Total PVR increased by twofold in our studies, which suggests the pruning of pulmonary vessels. While we did not carry out a histological analysis, Yin et al. did in MCT-treated

animals after four weeks of injections. In their histological analysis of the lungs, the pulmonary arterioles showed marked lesions (i.e. thickening, narrowed, and inflamed arterioles[18]), all consistent with characteristics found in PAH patients.

Ventricular contractility and stiffness in PAH cannot be explained by morphological changes alone

SV could only be maintained after two weeks of MCT treatment by the significant increase in end-systolic elastance. Increase in E_{es} has been previously reported to increase by Yin et al. (from 0.67 ± 0.12 to 0.95 ± 0.42 mmHg/μL),[18] de Man et al. (from 0.2 to 0.5 mmHg/μL),[33] and Blaudszun et al. (from 0.24 ± 0.12 to 0.56 ± 0.33 mmHg/μL)[34] from normo- to hypertensive states in MCT-models of PAH in rats. The model analysis showed that wall thickening and geometric remodeling alone were unable to explain all of the increased chamber elastance. The RV model used to predict ESPVR underestimates the data measured at ES of the PAH2, PAH3, and PAH4 groups unless the material parameters were adjusted and the maximal isometric tension T_{max} is increased by twofold. Predicted peak systolic stress-strain relations showed that intrinsic myocardial contractility increased significantly by week 2 and remained significantly higher than the control group. Rain et al.[1] found that active tension of RV myocytes from PAH patients was higher than those of normotensive subjects. Interestingly, CO in the PAH group was lower than the control group but without reaching statistical significance. Sabourin et al. studied RV cardiomyocytes from a three-week rat MCT model of PAH and in this group of hypertrophied RV myocytes found an increase in the expression of SERCA2 and the amplitude of calcium transients, which resulted in an increase in contractility. This would explain the results from our model analysis and Rain et al.'s measurements in samples from PAH patients. Sabourin et al. concluded that enhanced SR calcium load was mediated by STIM1L and TRPCs/Orail. The parallel in these studies indicates that MCT is a valuable model of PAH for mimicking the initial RV adaptation found in PAH patients.[2]

In our study, we observed a transient decrease in E_{ed} after one week of PAH, followed by a recovery to control values during PAH progression. The RV model analysis suggests that this initial decrease was due to a temporary increase in myocardial compliance. This myocardium intrinsic change, along with RV wall thickening as hypertrophy progressed, contributed to the restoration of end-diastolic chamber stiffness subsequently. The temporary increase in diastolic myocardial compliance followed by the subsequent increase in ED pressure contributed significantly to the maintenance of SV via the Frank-Starling mechanism by increasing end-diastolic volume. In humans with PAH, RV diastolic stiffness E_{ed} has been shown to be sensitive to the stage of the disease. Trip et al. reported an increase in E_{ed} from control ($\sim$0.25 mmHg/mL) to PAH patients.[3] In their

study, they determined that diastolic stiffening of the RV is independent of the systolic adaptation process. They also suggested that E_{ed} increment in PAH patients with a survival > 5 years may be explained by the hypertrophy of the RV, while in patients with < 5 years such increase may be related to additional intrinsic alterations of the myocardium. One possible mechanism of the acute loss of myocardial stiffness may be an increase in the fraction of the more compliant N2BA isoform of titin as a fraction of total titin, as was reported by Rain et al.[35] in rats after seven weeks of mild PA banding. While E_{ed} was not statistically different from the control and PAH4 groups, the model shows an increase in EDPVR stiffness and points towards stiffening of the passive sarcomere length-tension relation, which rose in PAH4.

Ventriculo-vascular coupling in PAH remains unaffected

Several studies have used η to evaluate the adaptation and performance of the RV during PAH. In a study carried out by de Man et al. in a MCT-induced PAH rat model, they reported a decrease in η from the control to severe disease state (from 1.0 to 0.5).[33] Even though Yin et al. used the same animal model, they reported no change in η when comparing normo- to hypertensive MCT rats (control: $η = 1.44 \pm 0.08$, PAH: $η = 1.42 \pm 0.33$).[18] Our outcomes showed that the RV and the pulmonary arteries are coupled through the disease progression, indicating that the heart is still keeping up with the high-pressure overload. Here, we found a hypertrophic heart, with an increase in ES volume and ED volume but a preserved SV, no change in CO, EF nor HR. CO is preserved even though the resting volume of the RV increased. This supports the claim that the RV is still in the adapting phase and working along the increase in PA pressures.

Limitations

Hemodynamic measurements were carried out using isoflurane as an anesthetic during open-chest surgery. Some studies have shown that isoflurane can affect hemodynamics measurements by reducing PAP, total PVR, and contractility.[36,37] Ewalenko et al. demonstrated that while true that pulmonary vascular tone decreased with isoflurane compared to propofol, this decrease was negligible and did not affect impedance. Given that all animals underwent the same in-vivo measurements, and there was a statistically significant difference in mPAP and total PVR across the groups, we think that the effects of isoflurane can be neglected. Open-chest surgeries may produce an artifactual reduction of right ventricular pressure.[38] Pacher et al. have shown that it is feasible to obtain similar results in open- vs. closed-chest surgery, if body temperature, fluid balance, and anesthesia are adequately regulated and monitored during the surgical procedure,[5] which we carefully monitored in our experiments. Given that the study focused on RV mechanics

and hemodynamics and relied on the literature for expected biological changes, no biological data are presented.

Although the RV wall is not a membrane and the thin-walled assumption is less well justified when the wall thickens in PAH, the wall thickness to radius ratio did not exceed 0.14, and the model was only used to estimate global pressure-volume relations not non-homogeneous myocardial stress distributions. To compute RV end-diastolic and end-systolic pressure-volume relations from RV geometry and myocardial resting and active material properties, a spherical model of the RV was adapted from the more comprehensive biventricular TriSeg model.[37] Like previous works,[12,13] our model includes length-dependent calcium-sensitivity mechanics. However, we simplified the TriSeg model to exclude the LV, ventricular interactions, and circulatory dynamics because the current study was only focused on the effects of RV geometry and material properties on PV relations and because all the hemodynamic and structural data necessary to parameterize the more comprehensive model were not measured. In spite of these simplifications, the model was able to recapitulate the experimentally measured mean RV pressure-volume relations, using sarcomere length-tension relations similar to those reported in rat cardiac trabeculae by ter Keurs et al.[16]

Conclusion

In conclusion, these results suggest the MCT-animal model at four weeks at 60 mg/kg is a model of RV compensation. At week 1, SV was maintained by the RV decreasing its diastolic chamber stiffness, not via changes in systolic function. However, by week 2 that mechanism was not enough: diastolic function had reversed closer to baseline and increased contractility was needed as the RV pressures started to rise. Changes in the EDPVR (i.e. decrease in passive tension) could also be an effect of monocrotaline as there was no change/increase in pressure. By week 2, however, the RV contractility increases (increase in active sarcomere tension) in order to maintain SV and CO. Interestingly, by weeks 3 and 4, the RV does not appear to need to recruit as much muscle fibers because the ventricle started to remodel. Hence, the effects of geometric remodeling on the EDPVR and of increased myocardial contractility on the ESPVR were the major mechanisms by which SV was preserved in the setting of elevated PAP, and both mechanisms contributed equally during weeks 2–4. Therefore, compensated right ventricular function depends on chamber remodeling and contractile augmentation in the onset of PAH in this rat animal model.

References

1. Hoeper MM, Bogaard HJ, Condliffe R, et al. Definitions and diagnosis of pulmonary hypertension. *J Am Coll Cardiol* 2013; 62(25): D42–50.

2. Rain S, Handoko ML, Trip P, et al. Right ventricular diastolic impairment in patients with pulmonary arterial hypertension. *Circulation* 2013; 128(18): 2016–2025.

3. Trip P, Rain S, Handoko ML, et al. Clinical relevance of right ventricular diastolic stiffness in pulmonary hypertension. *Eur Respir J* 2015; 45: 1603–1612.

4. Vanderpool RR, Pinsky MR, Naeije R, et al. RV-pulmonary arterial coupling predicts outcome in patients referred for pulmonary hypertension. *Heart* 2015; 101(1): 37–43.

5. Pacher P, Nagayama T, Mukhopadhyay P, et al. Measurement of cardiac function using pressure-volume conductance catheter technique in mice and rats. *Nat Protoc* 2008; 3(9): 1422–1434.

6. Wang Z, Schreier DA, Hacker TA, et al. Progressive right ventricular functional and structural changes in a mouse model of pulmonary arterial hypertension. *Physiol Rep* 2013; 1(7): e00184.

7. Langer SFJ, Habazettl H, Kuebler WM, et al. Estimation of the left ventricular relaxation time constant tau requires consideration of the pressure asymptote. *Physiol Res* 2005; 54(6): 601–610.

8. Shintani H and Glantz SA. The left ventricular diastolic pressure-volume relation, relaxation and filling. In: Gaasch WH and LeWinter MM (eds) *Left ventricular diastolic dysfunction and heart failure*. Philadelphia, PA: Lea & Febinger, 1994, pp.57–88.

9. Zeineh NS, Bachman TN, El-Haddad H, et al. Effects of acute intravenous iloprost on right ventricular hemodynamics in rats with chronic pulmonary hypertension. *Pulm Circ* 2014; 4(4): 612–618.

10. Bellofiore A and Chesler NC. Methods for measuring right ventricular function and hemodynamic coupling with the pulmonary vasculature. *Ann Biomed Eng* 2013; 41(7): 1384–1398.

11. Lee LC, Zhihong Z, Hinson A, et al. Reduction in left ventricular wall stress and improvement in function in failing hearts using Algisyl-LVR. *J Vis Exp* 2013; 8(74): 1–6.

12. Vinnakota KC and Bassingthwaighte JB. Myocardial density and composition: a basis for calculating intracellular metabolite concentrations. *Am J Physiol Circ Physiol* 2004; 286(5): H1742–1749.

13. Arts T, Delhaas T, Bovendeerd P, et al. Adaptation to mechanical load determines shape and properties of heart and circulation: the CircAdapt model. *Am J Physiol Circ Physiol* 2005; 288(4): H1943–1954.

14. Zhang X, Haynes P, Campbell KS, et al. Numerical evaluation of myofiber orientation and transmural contractile strength on left ventricular function. *J Biomech Eng* 2015; 137(4): 044502.

15. Guccione JM, Waldman LK and McCulloch AD. Mechanics of active contraction in cardiac muscle: Part II–Cylindrical models of the systolic left ventricle. *J Biomech Eng* 1993; 115(1): 82–90.

16. ter Keurs HE, Rijnsburger WH, van Heuningen R, et al. Tension development and sarcomere length in rat cardiac trabeculae. Evidence of length-dependent activation. *Circ Res* 1980; 46(5): 703–714.

17. Handoko ML, de Man FS, Happé CM, et al. Opposite effects of training in rats with stable and progressive pulmonary hypertension. *Circulation* 2009; 120(1): 42–49.

18. Yin X, Wang L, Qin G, et al. Rats with chronic, stable pulmonary hypertension tolerate low dose sevoflurane inhalation as well as normal rats do. *PLoS One* 2016; 11(5): e0154154.

19. Werchan PM and Mcdonough H. Right ventricular performance after pulmonary hypertension. *In Vitro* 1989; 130(23): 1328–1336.

20. Umar S. *Molecular and cellular characterization of cardiac overload-induced hypertrophy and failure* (Doctoral Thesis). Leiden University, 2009, Chapter 7, pp. 165–172.

21. Correia-Pinto J, Henriques-Coelho T, Roncon-Albuquerque R, et al. Time course and mechanisms of left ventricular systolic and diastolic dysfunction in monocrotaline-induced pulmonary hypertension. *Basic Res Cardiol* 2009; 104(5): 535–545.

22. Gomez-Arroyo JG, Farkas L, Alhussaini AA, et al. The monocrotaline model of pulmonary hypertension in perspective. *Am J Physiol Lung Cell Mol Physiol* 2012; 302(4): L363–369.

23. Abe K, Toba M, Alzoubi A, et al. Formation of plexiform lesions in experimental severe pulmonary arterial hypertension. *Circulation* 2010; 121: 2747–2754.

24. Umar S, Lee J-H, de Lange E, et al. Spontaneous ventricular fibrillation in right ventricular failure secondary to chronic pulmonary hypertension. *Circ Arrhythmia Electrophysiol* 2012; 5(1): 181–190.

25. Alencar A, Carvalho F, Silva AM, et al. Synergistic interaction between a PDE5 inhibitor (sildenafil) and a new adenosine A 2A receptor agonist (LASSBio-1359) improves pulmonary hypertension in rats. *PLoS One* 2018; 13(4): e0195047.

26. White RJ, Meoli DF, Swarthout RF, et al. Plexiform-like lesions and increased tissue factor expression in a rat model of severe pulmonary arterial hypertension. *Am J Physiol Lung Cell Mol Physiol* 2007; 293: 583–590.

27. Schermuly RT, Kreisselmeier KP, Ghofrani HA, et al. Chronic sildenafil treatment inhibits monocrotaline-induced pulmonary hypertension in rats. *Am J Respir Crit Care Med* 2004; 169(1): 39–45.

28. Hessel MHM, Steendijk P, den Adel B, et al. Characterization of right ventricular function after monocrotaline-induced pulmonary hypertension in the intact rat. *Am J Physiol Heart Circ Physiol* 2006; 291(5): H2424–2430.

29. Benoist D, Stones R, Drinkhill M, et al. Arrhythmogenic substrate in hearts of rats with monocrotaline-induced pulmonary hypertension and right ventricular hypertrophy. *Am J Physiol Circ Physiol* 2011; 300(6): H2230–2237.

30. Hardy MEL, Pervolaraki E, Bernus O, et al. Dynamic action potential restitution contributes to mechanical restitution in right ventricular myocytes from pulmonary hypertensive rats. *Front Physiol* 2018; 9(March): 1–11.

31. Vaillancourt M, Chia P, Sarji S, et al. Autonomic nervous system involvement in pulmonary arterial hypertension. *Respir Res* 2017; 18(1): 201.

32. Benoist D, Stones R, Drinkhill MJ, et al. Cardiac arrhythmia mechanisms in rats with heart failure induced by pulmonary

hypertension. *Am J Physiol Circ Physiol* 2012; 302(11): H2381–2395.

33. de Man FS, Handoko ML, van Ballegoij JJM, et al. Bisoprolol delays progression towards right heart failure in experimental pulmonary hypertension. *Circ Heart Fail* 2012; 5(1): 97–105.

34. Blaudszun G and Morel DR. Superiority of desflurane over sevoflurane and isoflurane in the presence of pressure-overload right ventricle hypertrophy in rats. *Anesthesiology* 2012; 117(5): 1051–1061.

35. Handoko ML, De Man FS, Happé CM, et al. Opposite effects of training in rats with stable and progressive pulmonary hypertension. *Circulation* 2009; 120(1): 42–49.

36. Cheng DC and Edelist G. Isoflurane and primary pulmonary hypertension. *Anaesthesia* 1988; 43(1): 22–24.

37. Ewalenko P, Brimioulle S, Delcroix M, et al. Comparison of the effects of isoflurane with those of propofol on pulmonary vascular impedance in experimental embolic pulmonary hypertension. *Br J Anaesth* 1997; 79: 625–630.

38. Provencher S, Archer SL, Ramirez FD, et al. Standards and methodological rigor in pulmonary arterial hypertension preclinical and translational research. *Circ Res* 2018; 122(7): 1021–1032.